Journal of Integrative Neuroscience

J. Integr. Neurosci. **2026**; 25(4): 50023
https://doi.org/10.31083/JIN50023

Original Research

FPS-ZM1 Exerts Neuroprotection in Cardiac-Arrest Mice through Inhibiting Oxidative Stress and Pyroptosis via the HMGB1/RAGE Axis

Ying Zhu[1,2], Qianhui Lin[1,2], Yanping Wu[1,2], Jing Hou[1,2], Liping Lu[1,2], Song Xu[1,2], Ling Li[1,2], Zhui Yu[1,*]

[1]Department of Critical Care Medicine, Renmin Hospital of Wuhan University, 430060 Wuhan, Hubei, China
[2]Central Laboratory, Renmin Hospital of Wuhan University, 430060 Wuhan, Hubei, China
*Correspondence: yuzhui@whu.edu.cn (Zhui Yu)
Academic Editor: Bettina Platt
Submitted: 14 January 2026 Revised: 11 February 2026 Accepted: 5 March 2026 Published: 17 April 2026

Abstract

Background: Cardiac arrest (CA) is a widespread public health problem with high mortality, severe neurological sequelae, and limited pharmacological therapies. We investigated the neuroprotective effect of a novel drug, FPS-ZM1 (FPS), on CA and explored its potential mechanism. **Methods**: A potassium chloride–induced CA was induced for 9.5 min in mice, with i.p. injections of FPS or vehicle administered 24 and 1 h before induction. Postoperative assessments included survival rate, body weight change, neurological scores, and neuronal pathological damage. The expression levels of the high mobility group box 1 (HMGB1)/receptor for advanced glycation end products (RAGE) axis, pyroptosis-related molecules, oxidative stress markers, and the nuclear factor erythroid 2-related factor 2 (Nrf2)/heme oxygenase-1 (HO-1) axis were evaluated. **Results**: Post-CA brain injury (PCABI) activated the HMGB1/RAGE axis, triggering intensified oxidative stress and aggravated pyroptosis. In contrast, pretreatment with FPS attenuated CA-induced injuries. FPS pretreatment was found to suppress the activation of the HMGB1/RAGE axis, alleviate pyroptosis and the release of associated inflammatory mediators, and enhance the Nrf2/HO-1 antioxidant axis after PCABI. **Conclusion**: FPS pretreatment mitigated PCABI by concurrently modulating the HMGB1/RAGE inflammatory axis and the Nrf2/HO-1 antioxidant pathway, suggesting that RAGE antagonism represents a promising therapeutic strategy for PCABI.

Keywords: cardiac arrest; FPS-ZM1; HMGB1 protein; oxidative stress; pyroptosis; receptor for advanced glycation end products

1. Introduction

Cardiac arrest (CA) is characterized by high morbidity, low survival rates (typically <10%), and elevated mortality and disability outcomes [1]. Cardiopulmonary resuscitation (CPR) and defibrillation have enhanced the likelihood of initial resuscitation after CA [2], but vulnerability of the cerebrovascular system to hypoxia often leads to poor neurological outcomes. Although the brain constitutes a relatively small portion of the body, it receives about 20% of the cardiac output and is highly susceptible to ischemia/reperfusion injury (IRI) [3,4]. Post-CA brain injury (PCABI) affects nearly 80% of individuals who initially survive cardiac arrest, often resulting in coma, significant neurological sequelae, or death [5]. At present, international resuscitation guidelines advocate targeted temperature management (TTM) as the sole neuroprotective approach for managing PCABI after out-of-hospital CA [6,7]. However, the outcomes of these interventions have demonstrated limited success in both preclinical studies and clinical trials [5]. However, despite early animal studies suggesting neuroprotective potential, the large TTM1 and TTM2 clinical trials failed to demonstrate a clear benefit of TTM in the broader PCABI population [8,9]. Those findings showed the limitations of current treatment strategies and underscored the highly complex and incompletely elucidated pathophysiology of PCABI. Therefore, the identification of novel therapeutic targets or pharmacological interventions to attenuate CA-induced brain injury and improve neurological outcomes has become a critical and urgent research priority.

High mobility group box 1 (HMGB1) is an evolutionarily conserved protein found in multiple species, including both humans and rodents. It is widely expressed throughout the body, with significant expression in brain tissue [10]. Under normal physiological conditions, HMGB1 is essential for the formation of neuronal synapses, damage repair, and cellular homeostasis [10,11]. In response to cerebral injuries, such as hypoxia and ischemia, HMGB1 is released into the extracellular space, where it acts as a damage-associated molecular pattern (DAMP). Once released into the extracellular space, HMGB1 binds to pattern-recognition receptors, including the receptor for advanced glycation end products (RAGE) and toll-like receptor 4, potentially triggering sterile inflammation [12,13]. RAGE, the first identified high-affinity receptor for HMGB1 [14], exhibits increased expression that is primarily associated with exacerbated neuroinflammation after brain injury [15]. Research involving both human clinical trials and animal models has demonstrated increased concentrations of HMGB1 in the blood and cere-

brospinal fluid of individuals undergoing CA. These elevated levels correlated significantly with adverse neurological outcomes, suggesting that HMGB1 acts as a potential prognostic biomarker [16–18]. Furthermore, increased HMGB1 expression in serum and brain tissue in post-CA rats modulates the inflammatory response [18,19]. Given that RAGE is persistently activated after hypoxic-ischemic brain injury, thereby inducing neuroinflammation [20,21], inhibiting the HMGB1/RAGE axis theoretically represents a potentially effective therapeutic strategy for PCABI.

Pyroptosis is an inflammation-driven subtype of programmed cell death that occurs through activation of the inflammasome complex. The assembly of inflammasome complexes requires several key components, including apoptosis-associated speck-like protein containing a caspase recruitment domain (ASC) and pro-caspase 1. Upon activation, gasdermin D (GSDMD) is cleaved, resulting in the generation of transmembrane pores that disrupt cellular integrity. Consequently, inflammatory cytokines like interleukin-1 beta (IL-1β) and IL-18 are released, initiating a strong inflammatory response and cell death [22,23]. After ischemic brain injury, pyroptosis occurs in neurons, microglia, and astrocytes, among other cell types, and neutrophil extracellular traps are induced, contributing to irreversible brain damage [24,25]. Xu *et al*. [26] demonstrated that HMGB1 exerted its effects through RAGE-dependent endocytosis, subsequently triggering macrophage pyroptosis. Furthermore, previous studies have suggested that HMGB1 induces pyroptosis in endothelial cells and microglia via the HMGB1/RAGE/cathepsin B signaling pathway [27,28]. Although these findings are well-established, the specific role of pyroptosis in PCABI and the mechanisms by which drugs modulate this process are still not fully understood.

Nuclear factor erythroid 2-related factor 2 (Nrf2) plays a pivotal role in mediating the cellular antioxidant stress response and can activate the expression of multiple downstream antioxidant enzymes [29,30]. Heme oxygenase-1 (HO-1) is a classic downstream effector directly regulated by Nrf2; its expression is upregulated under various stress conditions and exerts pronounced antioxidant and anti-inflammatory effects [31]. Stimulation of the Nrf2/HO-1 signaling pathway has been shown to suppress brain IRI-associated oxidative stress and inflammatory responses, thereby exerting neuroprotection [32,33]. FPS-ZM1 (FPS), a non-toxic, high-affinity RAGE inhibitor, prevents RAGE from interacting with its ligands, including HMGB1 [34]. Shen *et al*. [35] showed that FPS enhanced Nrf2 and HO-1 expression, reduced oxidative stress in microglia, and thereby offered protection [36]. However, the effects of FPS administration on PCABI have not yet been fully elucidated.

We designed a series of experiments to evaluate the effects of FPS pretreatment on neurological outcomes in a cardiac arrest/cardiopulmonary resuscitation (CA/CPR) mouse model. Furthermore, we investigated the regulatory effects of FPS pretreatment on pyroptosis and oxidative stress, as well as the underlying mechanisms in PCABI.

2. Materials and Methods

2.1 Animals

Adult male C57BL/6 mice (aged 8–10 weeks, weighing 22–25 g) were sourced from Hunan SJA Laboratory Animal Co., Ltd. (Changsha, Hunan, China). Before the experiment, all mice were given at least one week to habituate to the colony room. During the study, the mice were kept under standardized conditions, with constant temperature and humidity control, a 12–12 h alternating light–dark cycle, and free access to standard rodent chow and water.

2.2 Randomization

Mice were randomly assigned to four experimental groups (n = 13/group) using a computer-generated randomization sequence to minimize selection bias: (1) Sham + vehicle; (2) Sham + FPS; (3) CA/CPR + vehicle; (4) CA/CPR + FPS. Randomization was performed by an investigator (QL) who was not involved in subsequent data analysis.

2.3 Blinding

One designated investigator (QL) was responsible for drug preparation and administration. All other investigators involved in surgical procedures, neurological function assessments, data collection, and statistical analysis remained blind to the group allocation throughout the entire experiment to minimize potential bias.

2.4 The CA model

The CA model was generated in accordance with the protocol described previously [33,37]. In brief (Fig. 1), mice were weighed to confirm adherence to standard weight parameters. Anesthesia was induced using 5% isoflurane (v/v; vol%; R510-22-10, RWD Life Science Co., Ltd., Shenzhen, Guangdong, China), followed by tracheal intubation. Anesthesia was maintained by mechanical ventilation delivering 1.0%–1.5% isoflurane (v/v; vol%); a gas evacuation apparatus (V101, RWD Life Science Co., Ltd.) was used to remove anesthetic exhaust. Mice were ventilated through the tracheal tube at a tidal volume ranging from 0.3 to 0.5 mL. Electrocardiogram (ECG) was continuously monitored using subcutaneously placed needle electrodes and a PowerLab 26T system (PL26T04; ADInstruments Pty Ltd., Bella Vista, New South Wales, Australia). Body temperature was kept at 37.0 $\pm$ 0.2 °C with the assistance of a heating pad and lamp, with regulation monitored by a rectal probe. For drug administration, a PE10 catheter (424701, Becton, Dickinson and Company, Franklin Lakes, NJ, USA) was placed into the right jugular vein. After a 50 µL flush with heparinized saline (9041-08-1, 0.9%, Sinopharm Chemical Reagent Co., Ltd., Shanghai, China), CA was triggered by injecting 0.5 M potassium

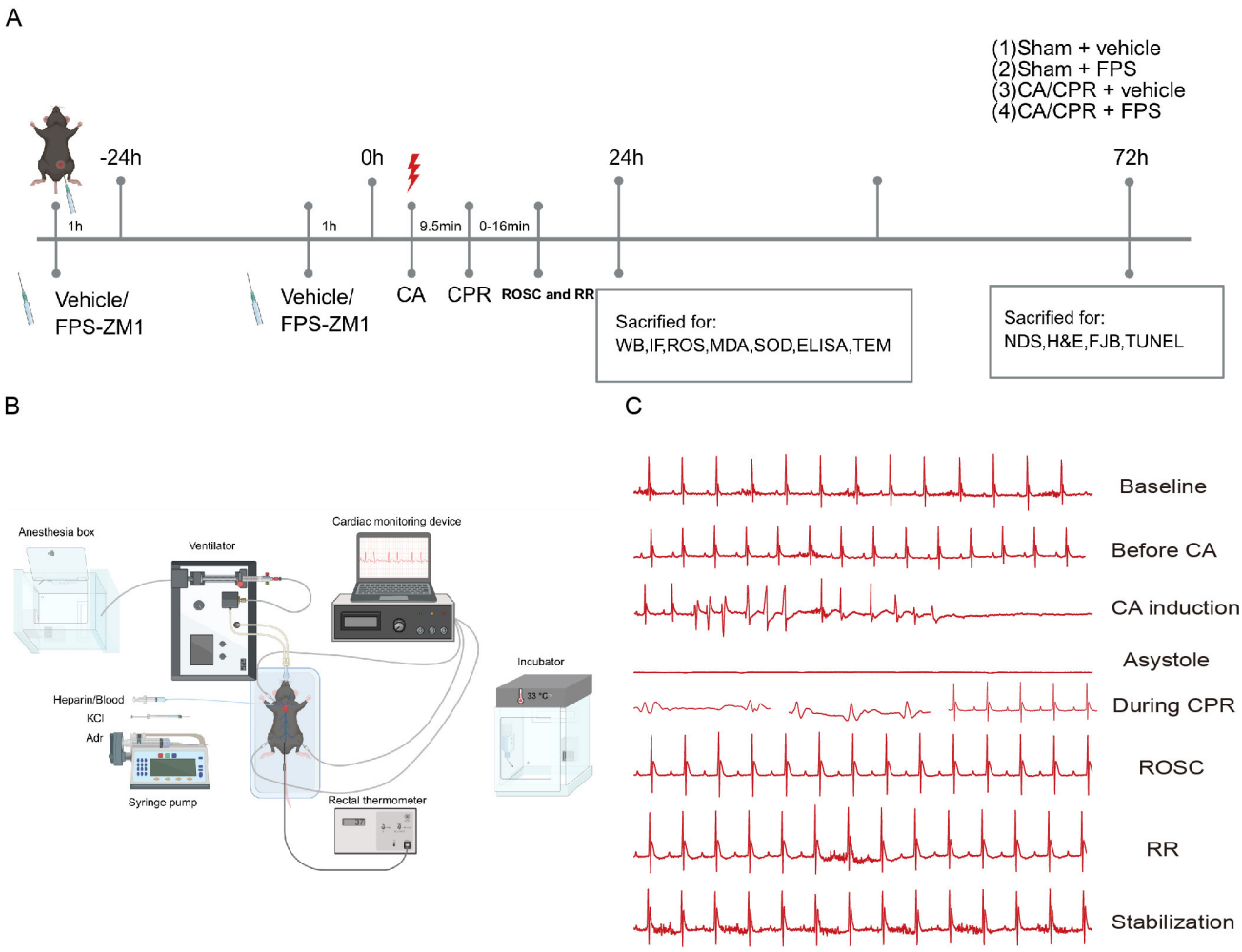

Fig. 1. Mouse experimental procedure. (A) Mice received CPR after 9.5 min of CA. FPS (RAGE inhibitor, 10 mg/kg) or an equivalent dose of vehicle (saline) was injected intraperitoneally on the day before surgery, and another dose again one h before CA. Impact of FPS on HMGB1/RAGE pathway modulation, as well as oxidative stress and pyroptosis-related signaling pathways induced by CA/CPR, was assessed 1 day after CA/CPR. The neuroprotective impact of FPS-ZM1 (FPS) was assessed 3 days after CA/CPR. Groups: (1) Sham + vehicle; (2) Sham + FPS; (3) CA/CPR + vehicle; (4) CA/CPR + FPS (n = 13/group). (B) The process of establishing a KCl-induced CA model in mice included the following steps: anesthesia; tracheal intubation; jugular vein catheterization; temperature and electrocardiogram monitoring; drug infusion; and postoperative targeted temperature management (TTM). (C) ECG monitoring was performed throughout the procedure, capturing representative waveform patterns. CA, cardiac arrest; CPR, cardiopulmonary resuscitation; ROSC, return of spontaneous circulation; RR, respiratory recovery; WB, Western Blot; IF, immunofluorescence; ROS, reactive oxygen species; MDA, malondialdehyde; SOD, superoxide dismutase; ELISA, enzyme-linked immunosorbent assay; NDS, neurological deficit score; H&E, Hematoxylin-eosin; FJB, Fluoro-Jade B; TUNEL, terminal deoxynucleotidyl transferase dUTP nick end labeling; KCl, potassium chloride; Adr, adrenaline; ECG, electrocardiogram; HMGB1, high mobility group box 1; RAGE, receptor for advanced glycation end products; TEM, transmission electron microscopy.

chloride (7447-40-7, [KCl], Sinopharm Chemical Reagent Co., Ltd.), 30 µL at 4 °C, followed by cessation of mechanical ventilation (MV). CA was verified by observing asystole on the ECG, cessation of spontaneous breathing, and the occurrence of urinary incontinence. Resuscitation was initiated 9.5 min after CA induction, and consisted of the resumption of mechanical ventilation with 100% oxygen, cessation of the warming protocol, and administration of 100 µL of epinephrine (61-76-7, 32 µg/mL, Sinopharm Chemical Reagent Co., Ltd.). Chest compressions were carried out at 300 beats/min. The return of spontaneous circulation (ROSC) was determined by the presence of a sustained sinus rhythm on the ECG. CPR was terminated if ROSC did not occur within 4 min. Upon the return of spontaneous respiration, the inspired gas mixture was gradually adjusted from 100% oxygen to a 1:1 oxygen-nitrogen ratio. After stabilization, independent respiration was achieved, and surgical sites were sutured. The tracheal tube was then

removed, and the mice were transferred to a thermal incubator set at 33.0 °C for a 2-h recovery period before being returned to their standard housing. Sham mice underwent identical anesthesia and surgical exposure of the jugular vein, but did not receive CA and CPR.

2.5 Drug Administrations and Experimental Design

Compound FPS (RAGE inhibitor, 10 mg/kg, HY-19370, MedChemExpress LLC, Monmouth Junction, NJ, USA) was administered via i.p. injection 24 h pre-surgery, and again 1 h before the surgical procedure. The dosing protocol for the administration was based on previous research findings [38]. Fig. 1A displays the experimental protocol.

2.6 Neurological Function Assessment

Neurological function was comprehensively assessed using two distinct scoring systems (**Supplementary Tables 1,2**). First, a 12-point scale [39] was used to assess the mice across six critical domains: responsiveness to stimuli; corneal reflex; respiration; righting reflex; coordination; and movement. Each domain was rated using a scale from 0 to 2, with 0 signifying severe impairment and 2 signifying normal function. Second, a 9-point grading scale [40] was used to evaluate neurological deficits based on motor performance. Mice were tested for their ability to climb a vertical grid, balance on a horizontal bar, and hang from a rope. Each task was scored from 0 to 3, where 0 represented severe disability and 3 represented normal function. Assessments were performed under standardized conditions (quiet room, consistent illumination, and minimal handling). Scoring was conducted independently by two investigators who were blind to group allocation and study hypotheses. When the discrepancy was $\geq$1 point, a third senior investigator with extensive experience in behavioral assessment re-evaluated the mouse, and the final score was determined based on the third rating and consensus.

2.7 Hematoxylin-Eosin (H&E) Staining

Abnormal neuronal morphology was evaluated through H&E staining. Mice were anesthetized by induction in an anesthesia box with 5% isoflurane with the inspired gas mixture at a 7:3 oxygen-nitrogen ratio. After the mice were anesthetized, intracardiac perfusion with 0.9% NaCl was performed, followed by fixation in 4% paraformaldehyde (PFA, G1101, Wuhan Servicebio Technology Co., Ltd., Wuhan, Hubei, China). The brains were fixed overnight at 4 °C in 4% PFA, then dehydrated and embedded in paraffin (Wuhan Servicebio Technology Co., Ltd.). Serial coronal sections (4 µm) were sliced, deparaffinized, stained using H&E, and examined under an Olympus microscope (Olympus Corporation, Hachioji-shi, Tokyo, Japan). Image analysis was performed using ImageJ2 (version 2.16.0, Laboratory for Optical and Computational Instrumentation, University of Wisconsin–Madison, Madison, WI, USA).

2.8 Nissl Staining

Nissl staining was used in order to quantify the density of cortical neurons. Brain tissue was extracted from anesthetized mice after decapitation and fixed in 4% PFA. After fixation, the specimens were embedded in paraffin and sectioned coronally at a thickness of 4 µm. The slices were then dewaxed, rehydrated, and stained by immersing them in a 0.2% cresyl violet solution (G1086, Wuhan Servicebio Technology Co., Ltd.) for 10 min. Images of the brain sections were obtained with an Olympus microscope. Nissl body counting was performed using ImageJ software.

2.9 Terminal Deoxynucleotidyl Transferase dUTP Nick End Labeling (TUNEL) Assay

The TUNEL assay was used to identify apoptotic neurons, according to the protocol included with the *In Situ* Cell-Death Detection Kit (PN0017, Wuhan Pinuofei Biotechnology Co., Ltd., Wuhan, Hubei, China). Paraffin-embedded brain-tissue sections were deparaffinized and subsequently exposed to proteinase K (Wuhan Pinuofei Biotechnology Co., Ltd.) to increase cellular membrane permeability. Thereafter, the sections were incubated with the TUNEL reaction solution at room temperature for 1 h to facilitate the detection process. After DAPI (Wuhan Pinuofei Biotechnology Co., Ltd.) staining to label the nuclei, the slides were then coverslipped using an anti-fade mounting medium (Wuhan Pinuofei Biotechnology Co., Ltd.). The tissue sections were examined under an Olympus microscope, and images were captured for quantification of cortical apoptotic cells per slide.

2.10 Fluoro-Jade B (FJB) Staining

FJB staining was used to evaluate neuronal degeneration and apoptosis. Brain sections were initially immersed in 0.06% potassium permanganate for 10 min, followed by incubation at room temperature for 20 min in 0.004% FJB solution (Merck Millipore, AG310, Merck Millipore, Darmstadt, Germany). After thorough rinsing and drying, the samples were coverslipped and analyzed using an Olympus microscope. The FJB-positive cell count within the cortical region was manually quantified using ImageJ software.

2.11 Immunofluorescent Staining

After deparaffinization, rehydration, and antigen retrieval, tissue sections were delineated and then treated with 3% bovine serum albumin (GC305010, Wuhan Servicebio Technology Co., Ltd.). Carefully prepared primary antibodies, sourced from the following suppliers, were then applied to the samples: HMGB1 (GB11103, Wuhan Servicebio Technology Co., Ltd.,1:500); RAGE (TC52809S, Abmart, Shanghai, China, 1:500); Nrf2 (#12721, Cell Signaling Technology, Danvers, MA, USA, 1:500); and caspase-1 (341030, Chengdu Zen Bioscience Co., Ltd., Chengdu, Sichuan, China, 1:500). The tissue slices were kept in a

humidified chamber and incubated at 4 °C overnight to ensure adequate antibody binding. Next, the samples were exposed to the corresponding secondary antibody (#4412 and #4408, Cell Signaling Technology, 1:1000) at room temperature for 1 h. Fluorescence intensity was analyzed with ImageJ software. HMGB1/RAGE colocalization analysis was as follows. Briefly, double immunofluorescence images were analyzed using ImageJ. For each group, three mice were included; for each mouse, three sections were analyzed, and one scanning field covering the cortical region per section was quantified. Within predefined cortical regions of interest (ROIs), HMGB1 and RAGE-positive cells were identified using a consistent thresholding strategy, and $HMGB1^{+}RAGE^{+}$ double-positive cells were confirmed on individual channels and merged images. Colocalization was quantified as the percentage of $HMGB1^{+}RAGE^{+}$ double-positive cells among total cells, with total cell number defined as the number of DAPI-positive nuclei within the ROI.

2.12 Transmission Electron Microscopy (TEM)

After cardiac perfusion with physiological saline, we immediately performed perfusion fixation using pre-chilled 2.5% glutaraldehyde fixative (G1102, Wuhan Servicebio Technology Co., Ltd.). The target cortical region was rapidly excised and sectioned into approximately 1 mm^3 cubes using a sharp blade. These were transferred into EP tubes containing the aforementioned fixative solution for post-fixation at 4 °C for 4–6 h. Ultrastructural alterations in mouse cortical neurons were imaged using a TEM (HT7700, Hitachi High-Tech Corporation, Tokyo, Japan). Neurons were identified by systematic scanning from low to high magnification based on ultrastructural characteristics.

2.13 Detection of Reactive Oxygen Species (ROS) Generation

After rapid cryopreservation in liquid nitrogen, brain tissue was embedded in OCT (G6059, Wuhan Servicebio Technology Co., Ltd.) and sliced coronally. To visualize ROS, sections were treated with dihydroethidium stain (D7008, Sigma-Aldrich, St. Louis, MO, USA) for 30 min at room temperature in darkness. Images were acquired with an Olympus microscope, and the fluorescence signals were analyzed and quantified using ImageJ software.

2.14 Malondialdehyde (MDA) Assay and Superoxide Dismutase (SOD) Assay

The level of lipid peroxidation was quantified using the MDA assay, and SOD activity was measured as an indicator of cellular capacity to neutralize ROS. Brain cortex samples were carefully dissected, homogenized in saline, and then subjected to centrifugation to obtain the supernatant. The activities of SOD and MDA were then assessed using commercial assay kits (A001-3-2 and A003-1-2, Nanjing Jiancheng Bioengineering Institute, Nanjing, Jiangsu, China) following the guidelines provided by the manufacturer.

2.15 Western Blot

To extract proteins, mouse brain cortex samples were extensively homogenized in a lysis buffer (G2002, Wuhan Servicebio Technology Co., Ltd.) using an ultrasonic cell processor (Ningbo Scientz Biotechnology Co., Ltd., Ningbo, Zhejiang, China). The extracted protein samples were combined with 5× loading buffer, heated at 95 °C for 5 min, and subjected to electrophoresis on 10–12% glycine gels (PG112-113, Epizyme Biotech Co., Ltd., Shanghai, China) for separation. The separated protein bands were transferred onto the polyvinylidene fluoride membrane (IPVH00010, Merck Millipore, Darmstadt, Germany). Membranes were blocked using either a rapid blocking buffer (PS108P, Epizyme Biotech Co., Ltd.) for 20 min or 5% skimmed milk powder in PBS for 1 h. Then they were exposed to the appropriate primary antibody and incubated overnight at 4 °C: HMGB1 (GB11103, Wuhan Servicebio Technology Co., Ltd., 1:1000); RAGE (TC52809S, Abmart, 1:1000); and caspase-1 (341030, Chengdu Zen Bioscience Co., Ltd., 1:500); gasdermin D (ER1907-37; HUABIO, Hangzhou, Zhejiang, China, 1:1000); Nrf2 (#12721, Cell Signaling Technology, 1:500); or HO-1 (ab68477, Abcam, Cambridge, UK, 1:500). After washing, the membranes were exposed to the respective secondary antibodies (#7074 and #7076, Cell Signaling Technology, 1:10,000) and maintained at room temperature for 1 h. To facilitate the detection of proteins with varying molecular weights, membranes were horizontally sectioned as needed. After three additional washes, protein signals were detected using an enhanced chemiluminescence (ECL) kit (HY-K1005, MedChemExpress LLC) and imaged with a Bio-Rad imaging system (Bio-Rad Laboratories, Inc., Hercules, California, USA). Protein expression levels were analyzed semi-quantitatively by ImageJ software.

2.16 Enzyme-Linked Immunosorbent Assay (ELISA)

Brain samples and peripheral blood were harvested in sterile tubes and stored at –80 °C. Levels of cytokine (IL-1β, IL-18, HMGB1, and RAGE) were quantified with the use of ELISA kits: Mouse HMGB1 (MU30043, Wuhan Bioswamp Biotechnology Co., Ltd., Wuhan, Hubei, China); RAGE (MU31640, Wuhan Bioswamp Biotechnology Co., Ltd.); IL-1β (JL18442, Shanghai Jianglai Industrial Co., Ltd., Shanghai, China); and IL-18 (JL20253, Shanghai Jianglai Industrial Co., Ltd.). Samples obtained after the previously described procedure were processed, with absorbance measured at 450 nm for all wells within each subgroup. The concentrations of cytokines were then determined by extrapolating values from the established standard curve.

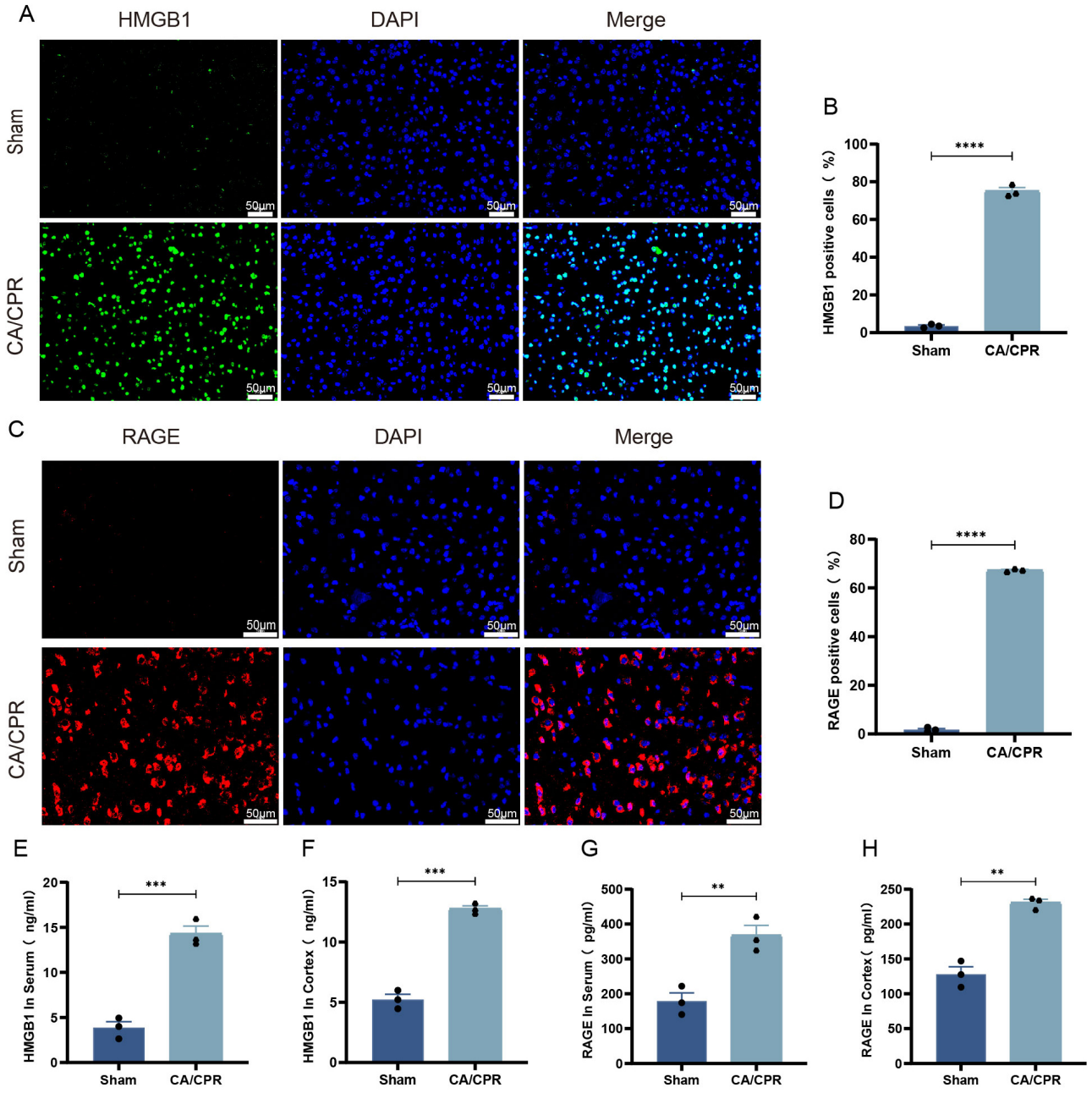

Fig. 2. The HMGB1/RAGE axis is activated by CA/CPR. (A) Typical immunofluorescence pictures of HMGB1. (B) Statistics of the proportion of HMGB1-positive cells across different groups. (C) Typical immunofluorescence pictures of RAGE. (D) Statistics of the proportion of RAGE-positive cells across different groups. (E,F) ELISA quantification of HMGB1 levels in serum and cortex in different groups. (G,H) ELISA quantification of RAGE levels in serum and cortex in different groups. Data are depicted as mean ± SEM. Scale bar = 50 μm (n = 3/group). ****$p < 0.0001$, ***$p < 0.001$, **$p < 0.01$. SEM, standard error of the mean.

2.17 Statistical Analysis

All collected experimental results were subjected to statistical analysis using GraphPad Prism (version 9.0.0.121, GraphPad Software, LLC, Boston, MA, USA), and the findings are presented as mean ± standard error of the mean (SEM). For comparisons between two groups, an independent two-tailed Student's t-test was used. For comparisons among multiple groups, one-way ANOVA was performed. When the ANOVA indicated an overall significant difference, Tukey's multiple comparisons test was applied for post-hoc pairwise comparisons across groups. Statistical significance was set at $p \leq 0.05$.

3. Results

3.1 The HMGB1/RAGE Axis was Activated by CA/CPR

To investigate alterations in RAGE and HMGB1 expression in mice after CA/CPR, cortical brain tissue and

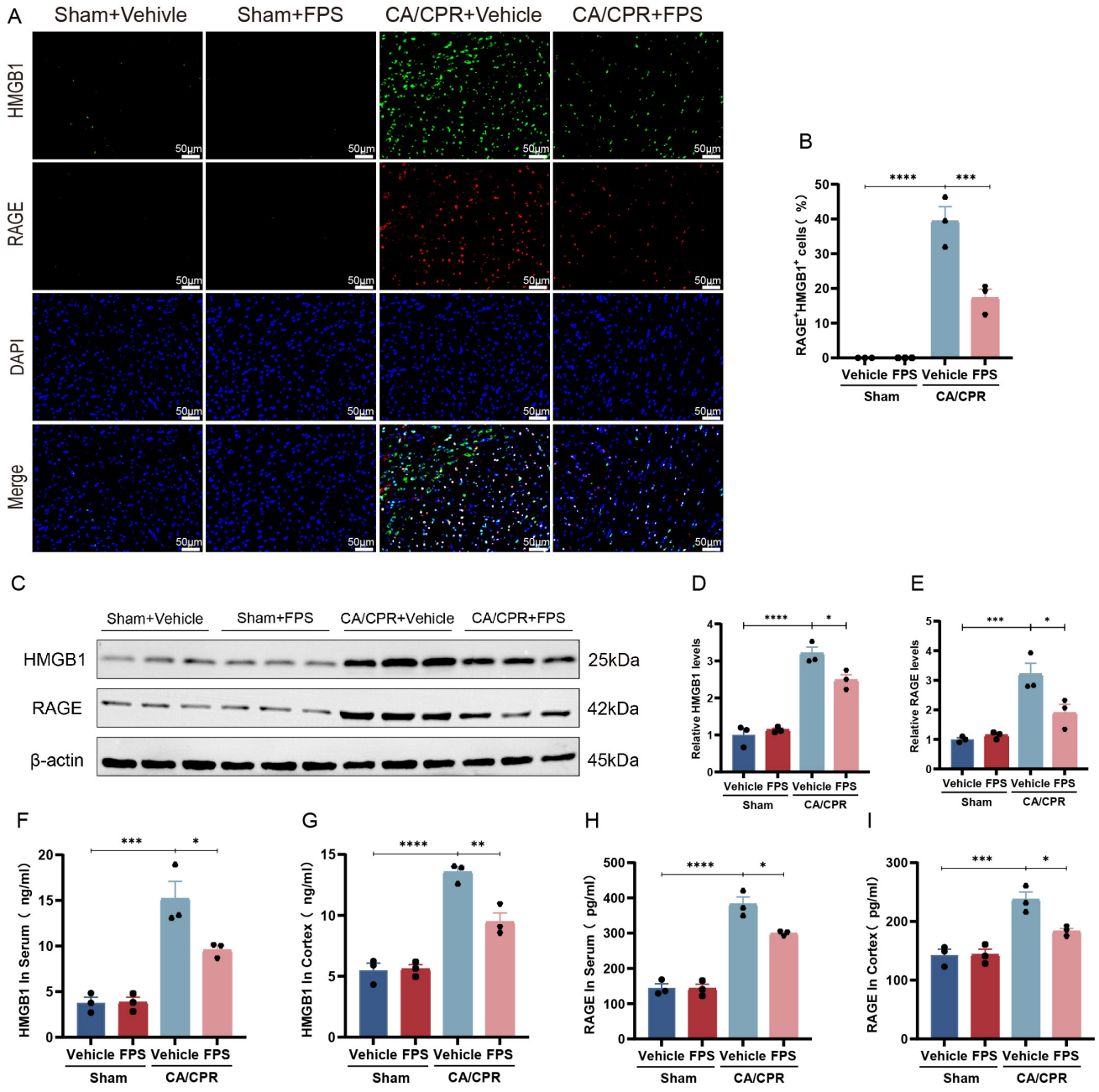

Fig. 3. FPS pretreatment prevented activation of the HMGB1/RAGE axis induced by CA/CPR. (A) Typical pictures of HMGB1 and RAGE double immunofluorescence staining. (B) Statistics of the proportion of HMGB1 and RAGE double-positive cells across different groups. (C) Typical protein immunoblotting bands of HMGB1 and RAGE. (D,E) Relative protein expression semiquantitative analysis of HMGB1 and RAGE across different groups. (F,G) ELISA quantification of HMGB1 levels in serum and cortex in different groups. (H,I) ELISA quantification of RAGE levels in serum and cortex in different groups. Data are depicted as mean ± SEM. Scale bar = 50 μm (n = 3/group). ****$p < 0.0001$, ***$p < 0.001$, **$p < 0.01$, *$p < 0.05$.

serum samples were analyzed using immunofluorescence and ELISA 24 h post-CA. Immunofluorescence results revealed a marked increase in RAGE and HMGB1 expression within the cerebral cortex of CA/CPR mice (Fig. 2A–D). Subsequent ELISA assays further confirmed that serum HMGB1 levels were significantly higher in the CA/CPR group than in the sham group (Fig. 2E,F). Similarly, serum RAGE levels were markedly higher in CA mice than in the sham group (Fig. 2G,H). These results indicated that both RAGE and HMGB1 were substantially upregulated during PCABI, suggesting activation of the HMGB1/RAGE axis and its potential involvement in the pathogenesis of PCABI.

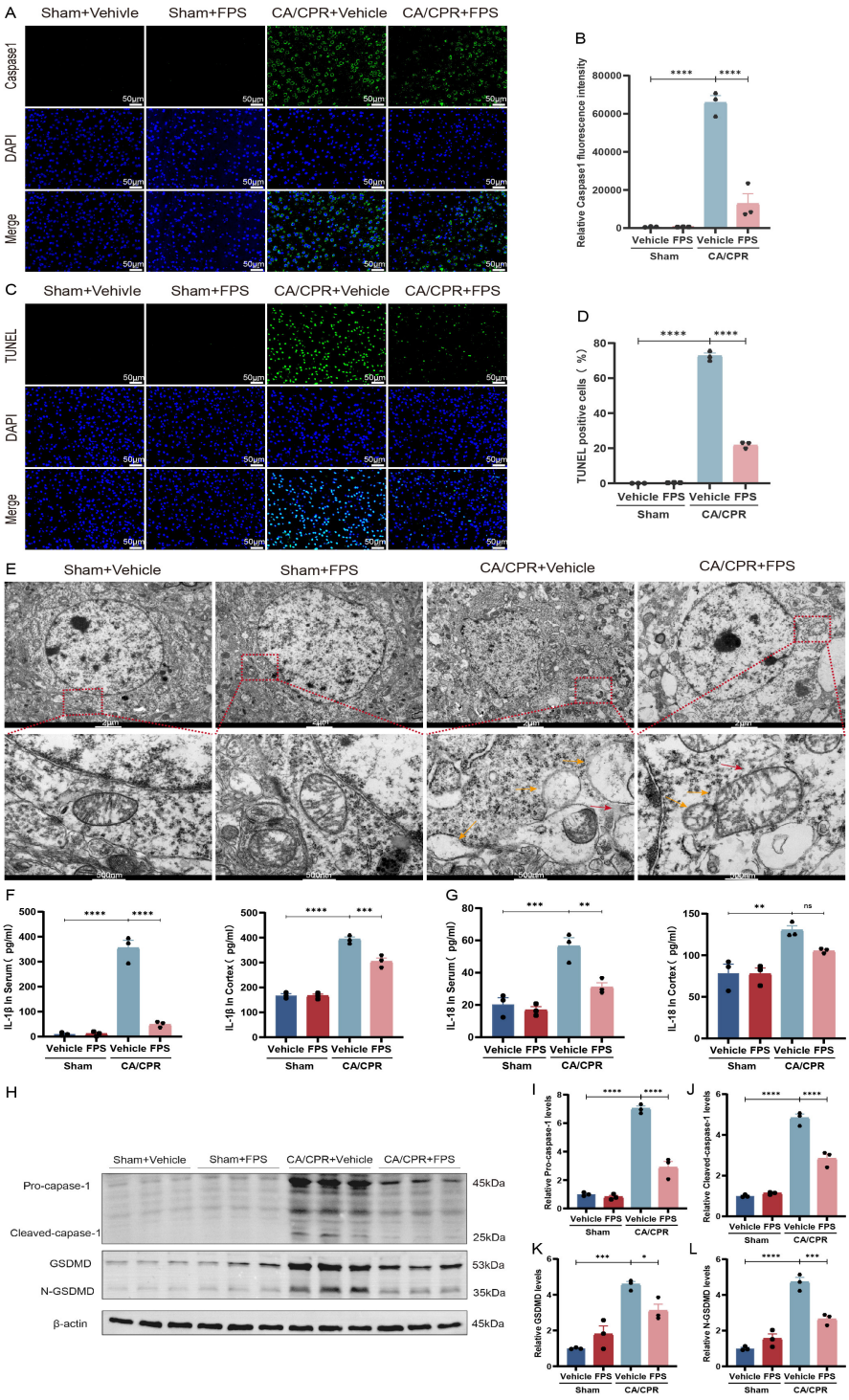

Fig. 4. FPS pretreatment attenuated the level of pyroptosis after CA/CPR. (A) Typical pictures of caspase-1 immunofluorescence staining. (B) Quantitative assessment of caspase-1 fluorescence intensity in different groups. (C) Typical pictures of TUNEL immunofluorescence staining. (D) Statistics of the proportion of TUNEL-positive cells in different groups. (E) Typical TEM pictures of cortical tissue (n = 3/group). Scale bar = 2 µm (low magnification) and 500 nm (high magnification). Arrows indicate pyroptotic neurons exhibiting cell membrane rupture (red) or organelle damage (orange). (F,G) ELISA quantification of the inflammatory cytokine IL-1β and IL-18 levels in serum and cortex in different groups. (H) Typical protein immunoblotting bands: Pro-caspase-1; cleaved-caspase-1; GSDMD; and N-GSDMD. (I–L) Relative protein expression semiquantitative analysis of pro-caspase-1, cleaved-caspase-1, GSDMD, and N-GSDMD in different groups. Data are depicted as mean ± SEM. Scale bar = 50 µm (n = 3/group). ****$p < 0.0001$, ***$p < 0.001$, **$p < 0.01$, *$p < 0.05$, ns: not significant. IL-1β, interleukin-1 beta; GSDMD, gasdermin D.

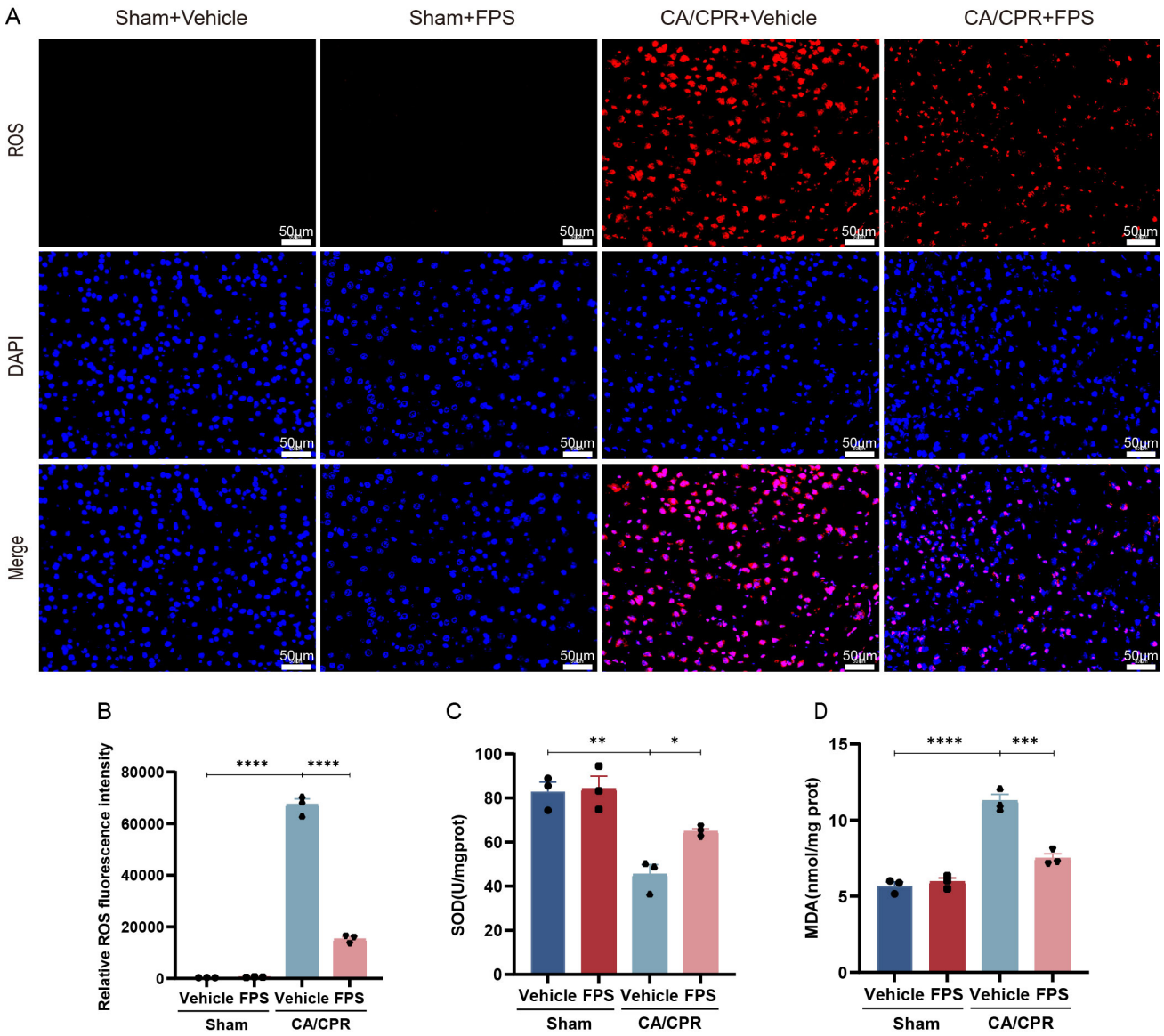

Fig. 5. FPS pretreatment reduced oxidative stress after CA/CPR. (A) Typical pictures of ROS immunofluorescence staining. (B) Quantitative assessment of ROS fluorescence intensity in different groups. (C,D) Evaluation of SOD activity and MDA levels. Data are depicted as mean ± SEM. Scale bar = 50 μm (n = 3/group). ****$p < 0.0001$, ***$p < 0.001$, **$p < 0.01$, *$p < 0.05$.

3.2 FPS Pretreatment Prevented Activation of the HMGB1/RAGE Axis Induced by CA/CPR

Although FPS is considered a specific RAGE inhibitor, the mechanistic basis for its suppression of RAGE activity in mouse brain tissue remains unclear. In the present study, immunofluorescence analysis revealed that, under physiological conditions, HMGB1 and RAGE exhibited only partial overlap in the mouse cerebral cortex, indicating a relatively low degree of colocalization (Fig. 3A). The CA/CPR + FPS group showed markedly less HMGB1/RAGE colocalization than did the CA/CPR + vehicle group ($p = 0.0009$, Fig. 3B). Consistent with the above observations, Western Blot analysis (Fig. 3C, the original Western blot image can be seen in the **Supplementary Material-Western Blot**) demonstrated significantly lower HMGB1 protein levels in cortex of the CA/CPR + FPS-pretreated group than in the CA/CPR + vehicle group ($p = 0.0299$, Fig. 3D), accompanied by a substantial decrease in RAGE protein levels (Fig. 3E). Furthermore, ELISA analysis revealed that HMGB1 and RAGE levels in both serum and cortex were significantly lower in the FPS–pretreated group than in the CA/CPR + vehicle group (Fig. 3F–I). Taken together, these findings suggested that FPS pretreatment exerted its effects, at least in part, by inhibiting CA/CPR-induced activation of the HMGB1/RAGE signaling pathway.

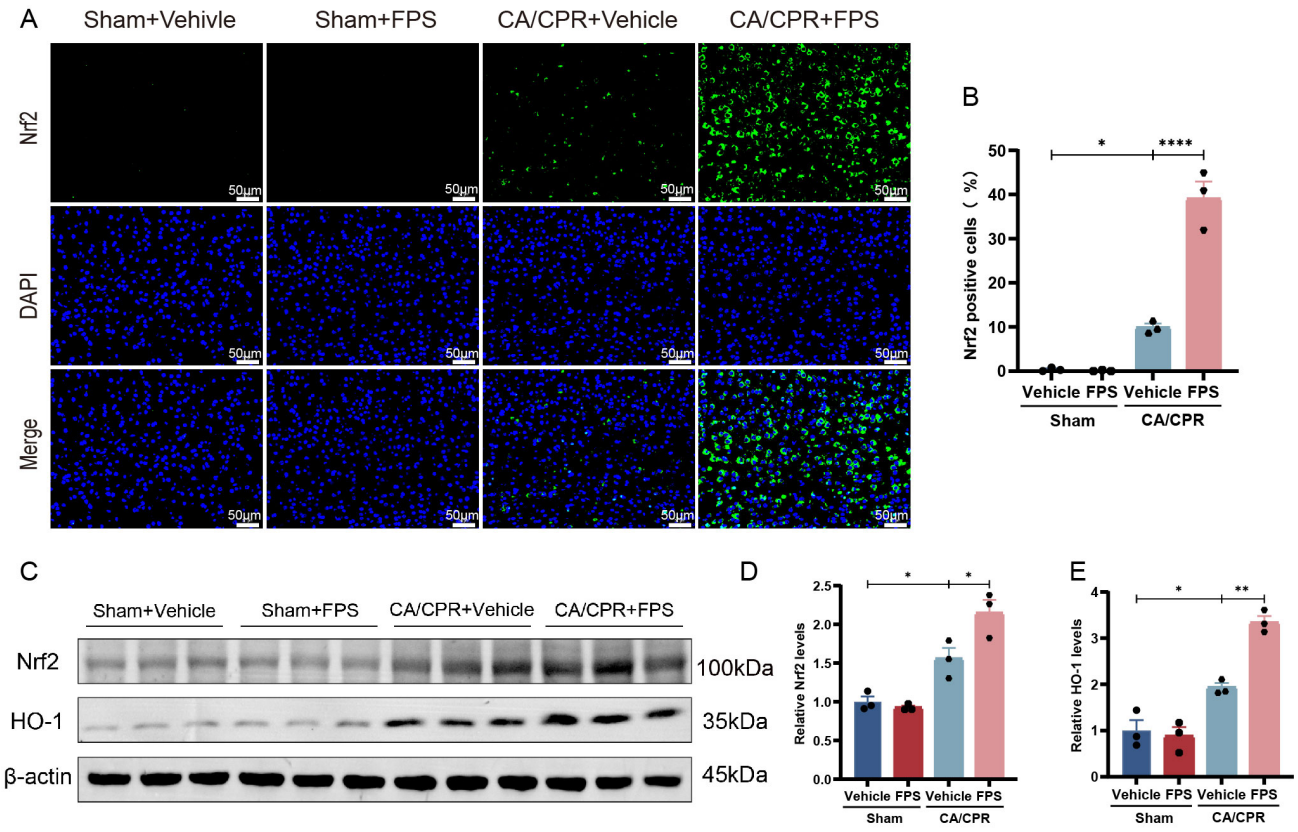

Fig. 6. FPS pretreatment upregulated Nrf2 and HO-1 expression after CA/CPR. (A) Typical pictures of Nrf2 immunofluorescence staining. (B) Statistics of the proportion of Nrf2-positive cells in different groups. (C) Typical protein immunoblotting bands of Nrf2 and HO-1. (D,E) Relative protein expression semiquantitative analysis of Nrf2 and HO-1 in different groups. Data are depicted as mean ± SEM. Scale bar = 50 μm (n = 3/group). ****$p < 0.0001$, **$p < 0.01$, *$p < 0.05$.

3.3 FPS Pretreatment Attenuated the Level of Pyroptosis After CA/CPR

Recent research has demonstrated that the HMGB1/RAGE axis is critically involved in mediating pyroptosis in neonatal hypoxic-ischemic brain injury and Kawasaki disease. Pretreatment with FPS has been shown to inhibit pyroptosis under these pathological conditions [27,28]. Building on these findings, the present study investigated whether FPS pretreatment could similarly attenuate CA/CPR-induced pyroptosis. Immunofluorescence (Fig. 4A–D) analysis revealed that, after CA/CPR, levels of activated caspase-1 and the proportion of TUNEL-positive cells in the mouse cerebral cortex were significantly increased. By contrast, FPS pretreatment markedly reduced activated caspase-1 levels and the number of TUNEL-positive cells. Notably, we used TUNEL as an indicator of DNA fragmentation and overall cell-death burden. To further explore pyroptosis, TEM revealed prominent ultrastructural cortical neuronal damage after CA/CPR, including membrane disruption, nuclear condensation, and severe organelle injury, which were alleviated by FPS pretreatment (Fig. 4E). As expected, ELISA (Fig. 4F,G) assays demonstrated that the concentrations of the cytokines IL-1β and IL-18 in the serum and brain tissue were significantly higher after CA/CPR. However, FPS pretreatment significantly blunted this increase. Protein analysis (Fig. 4H–L, the original Western Blot image can be seen in the **Supplementary Material-Western Blot**) showed that CA/CPR mice expressed higher levels of cleaved caspase-1 p20, GSDMD, and its N-terminal fragment N-GSDMD than did the sham group. It is important to note that FPS pretreatment substantially downregulated these protein levels. These results suggested that FPS pretreatment effectively suppressed CA/CPR-induced pyroptosis.

3.4 FPS Pretreatment Reduced Oxidative Stress After CA/CPR

To further elucidate the molecular mechanisms through which FPS mitigates PCABI, we measured oxidative stress levels induced by CA/CPR. As illustrated in Fig. 5A,B, immunofluorescence analysis demonstrated that CA/CPR significantly elevated ROS production in the cerebral cortex; whereas this effect was diminished by pretreatment with FPS. In addition, cortical SOD activity was markedly higher in the FPS-pretreated group than the CA/CPR + vehicle group (p = 0.0495, Fig. 5C), and accompanied by a substantial reduction in MDA levels (p =

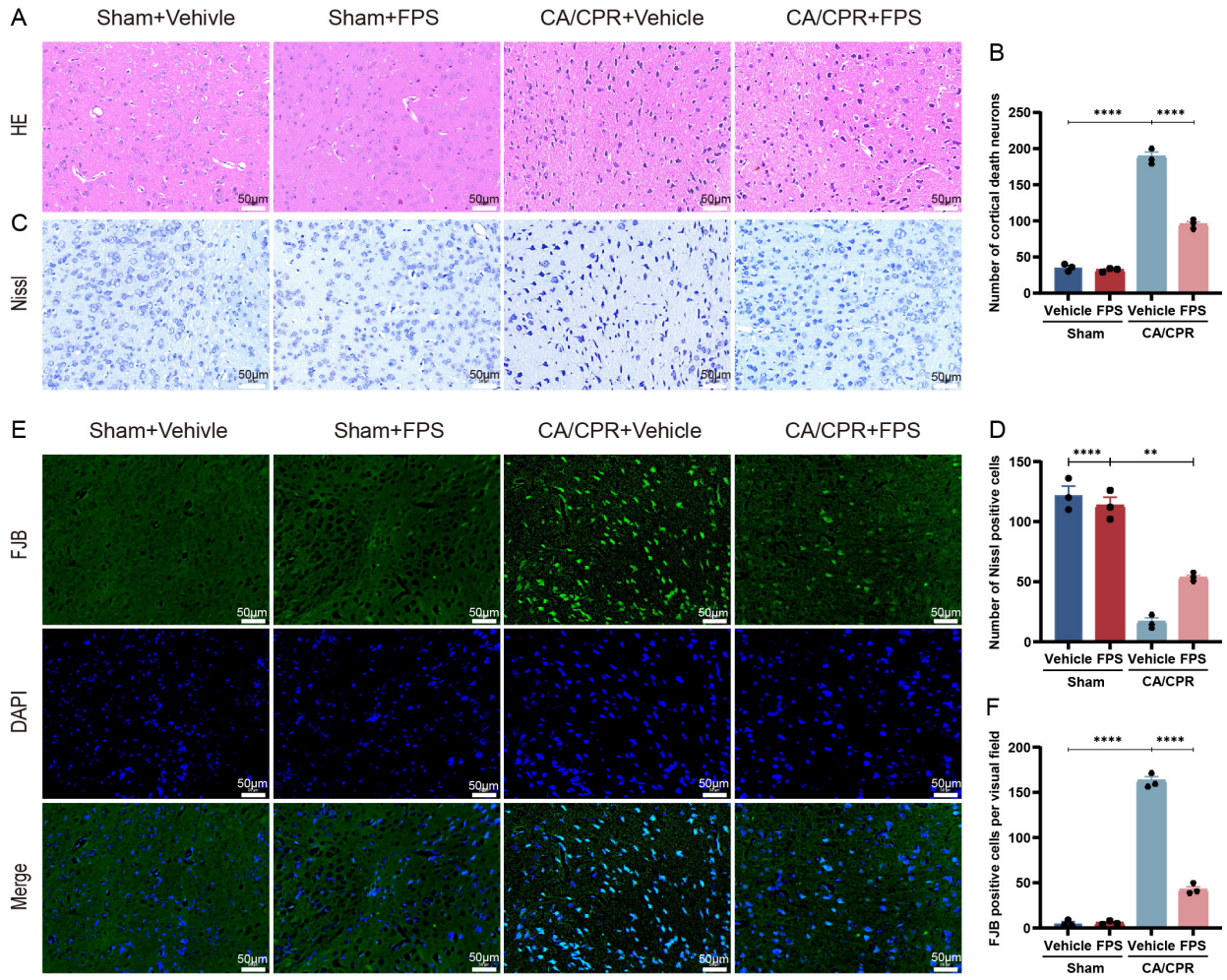

Fig. 7. FPS pretreatment reduced neuron damage after CA/CPR. The mouse brain cortex was stained with H&E, Nissl, and FJB 3 days after CA/CPR to assess neuropathological damage. (A) Typical pictures of H&E staining. (B) Number of dead cortical neurons. (C) Typical pictures of Nissl staining. (D) Quantification of Nissl-positive cells. (E) Typical pictures of FJB staining. (F) Quantification of FJB-positive cells. Data are depicted as mean ± SEM. Scale bar = 50 μm (n = 3/group). ****$p < 0.0001$, **$p < 0.01$.

0.0001, Fig. 5D). Collectively, these findings indicated that FPS pretreatment significantly alleviated CA/CPR-induced oxidative stress.

3.5 FPS Pretreatment Upregulated Nrf2 and HO-1 Expression After CA/CPR

Previous research demonstrated that FPS possesses antioxidant properties and can upregulate Nrf2 and HO-1 levels in a dose-dependent fashion, thereby providing protective effects [35]. Based on those findings, we hypothesized that FPS pretreatment attenuates CA/CPR-induced oxidative injury by modulating the Nrf2-HO1 axis. To examine changes in Nrf2 and its downstream antioxidant signaling, we performed immunofluorescence staining (Fig. 6A,B) and Western Blot analysis (Fig. 6C–E, the original Western Blot image can be seen in the **Supplementary Material-Western Blot**). Immunofluorescence examination revealed that Nrf2 expression exhibited a slight elevation after CA/CPR. This suggested that CA/CPR manipulation stimulated Nrf2 expression to a modest increase, although it did not produce a sufficient protective effect. Notably, FPS pretreatment markedly increased the overall Nrf2 protein signal after CA/CPR. Consistent with these findings, Western Blot analysis further confirmed that FPS pretreatment significantly upregulated total Nrf2 protein levels as well as the key downstream effector HO-1 after CA/CPR. Collectively, these results indicated that FPS pretreatment strongly enhanced Nrf2 protein expression after CA/CPR, accompanied by upregulation of the antioxidant protein HO-1. These results are consistent with the effect of FPS pretreatment in reducing oxidative stress, suggesting that the Nrf2/HO-1 signaling axis may be involved in its protective effect against oxidative stress after CA/CPR.

3.6 FPS Pretreatment Reduced Neuron Damage After CA/CPR

To further characterize the neuropathological alterations in the brain after CA/CPR, brain samples were har-

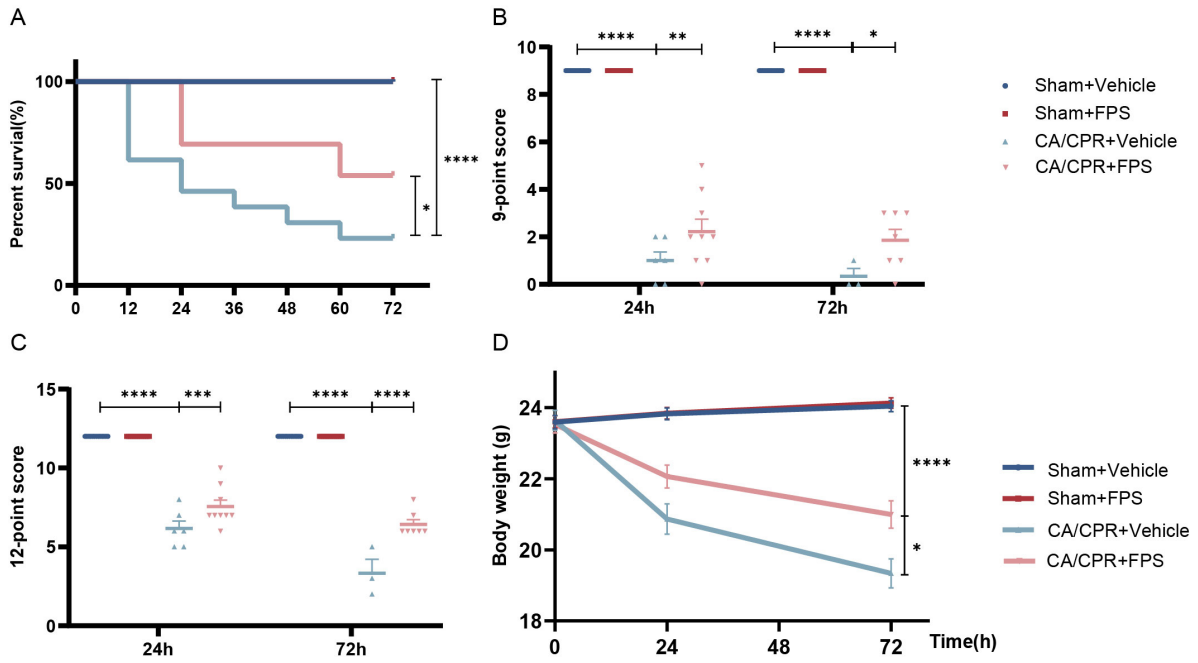

Fig. 8. FPS pretreatment ameliorated neurological function and survival after CA/CPR. (A) Survival percentage of mice was measured 3 days. Survival curves were generated using the Kaplan–Meier method and compared by the log-rank (Mantel–Cox) test. (B,C) 9-point and 12-point scoring systems at 1 and 3 days. (D) Body weight reduction in mice was observed at 1 and 3 days. Data are depicted as mean ± SEM (n = 13/group). ****$p < 0.0001$, ***$p < 0.001$, **$p < 0.01$, *$p < 0.05$.

vested on postoperative day 3 and subjected to H&E, Nissl, and FJB staining. The H&E (Fig. 7A,B) results showed that neurons in the sham group displayed clear, intact morphology. In contrast, the CA/CPR + vehicle group neurons were atrophied, with a reduced cytoplasmic volume, and nuclei and nucleoli were blurred. In the CA/CPR + FPS group, the majority of neurons retained relatively normal cytoplasmic and nuclear architecture, and only a small proportion of cells showed mild shrinkage, characterized by decreased cytoplasm and atypical nuclei. Nissl staining further demonstrated pronounced neuronal damage in the CA/CPR + vehicle group, characterized by pyknosis, karyorrhexis, and karyolysis, a notable loss of Nissl bodies, and a reduction in Nissl-positive neuronal counts compared with the sham group ($p < 0.0001$, Fig. 7C,D). Notably, FPS pretreatment resulted in a markedly higher count of Nissl-positive neurons than in the CA/CPR + vehicle group ($p = 0.0065$, Fig. 7C,D). FJB staining revealed a lower number of FJB-positive cells in the FPS pretreatment group, indicating less neuronal degeneration and better neuronal survival than in the CA/CPR + vehicle group ($p < 0.0001$, Fig. 7E,F). Taken together, these data showed that FPS alleviated PCABI and conferred a neuroprotective effect.

3.7 FPS Pretreatment Ameliorated Neurological Function and Survival After CA/CPR

Neurological outcomes after CA/CPR were assessed using 9- and 12-point neurological-function scoring systems. Body weight changes were monitored on days 1 and 3 after resuscitation, and survival rates were recorded daily. Survival analysis (Fig. 8A) showed that the FPS pretreatment group showed markedly better survival rates than did the CA/CPR + vehicle group, with higher survival rates at 1 day (69.23% vs. 46.15%), 2 days (69.23% vs. 30.77%), and 3 days (53.85% vs. 23.08%). Analysis of neurological-function scores indicated pronounced functional impairment in the CA/CPR group relative to the sham group at both time points. On the 9-point scale (Fig. 8B), the mean scores in the CA/CPR group were 1.00 on day 1 and 0.33 on day 3, whereas on the 12-point scale (Fig. 8C), the corresponding scores were 6.17 on day 1 and 3.33 on day 3. In contrast, mice receiving FPS pretreatment exhibited significantly better neurological performance than did the CA/CPR + vehicle group: the 9-point scores increased to 2.22 on day 1 ($p = 0.0079$) and 1.86 on day 3 ($p = 0.0128$), and the 12-point scores rose to 7.56 on day 1 ($p = 0.0005$) and 6.43 on day 3 ($p < 0.0001$). Furthermore, analysis of weight changes (Fig. 8D) revealed that mice in the FPS pretreatment group experienced significantly less weight loss than did the CA/CPR + vehicle group on both day 1 (1.46 g vs. 2.78 g, $p = 0.018$) and day 3 (2.53 g vs. 4.31 g, $p = 0.0109$). In summary, these data suggested that FPS improved neurological outcomes in mice after CA/CPR.

4. Discussion

In the present study, we demonstrated that the HMGB1/RAGE axis was activated after CA/CPR. Pharmacological inhibition of this axis with FPS pretreatment sig-

nificantly reduced pyroptosis, ROS accumulation, and suppressed the release of inflammatory mediators. These findings demonstrated that FPS exerted both anti-inflammatory and antioxidant actions. Additional experiments further indicated that the antioxidant properties of FPS might be mediated, at least in part, by activation of the Nrf2/HO-1.

The pathophysiology of PCABI consists of two phases: global cerebral ischemia and subsequent reperfusion after ROSC [41]. In the early phase of reperfusion, levels of ROS rise sharply, and ischemic necrotic neurons release large amounts of DAMPs. They are recognized by the innate immune system and trigger an inflammatory cascade that exacerbates PCABI [42,43]. Previous studies have shown that the binding of HMGB1 to its receptor, RAGE, activates multiple downstream signaling molecules, including nuclear factor kappa B (NF-κB), p38, and extracellular signal-regulated kinase 1/2 (ERK1/2) [44]. Moreover, excessive activation of RAGE promotes neuronal apoptosis [14]. Clinical evidence also supports the pivotal role of this pathway in brain injury: in patients with stroke, circulating levels of RAGE and HMGB1, as well as their interaction, are markedly elevated [14], and increased plasma concentrations of HMGB1 and the cleaved RAGE are closely associated with poor outcomes after ischemic brain injury [45,46]. Those findings suggest that the HMGB1/RAGE axis represents a critical regulatory node in ischemic brain injury. On this basis, we used a KCl-induced CA mouse model to evaluate changes in the HMGB1/RAGE axis after CA/CPR and their association with neurological outcomes. Our results showed that PCABI caused severe impairment of neural function. Concurrently, HMGB1 and RAGE were strongly co-expressed in cortical neurons, and their release levels in brain tissue and serum were significantly increased. By pharmacologically blocking the interaction between HMGB1 and RAGE, we found that CA-induced upregulation and increased release of HMGB1 and RAGE could be effectively reversed. Furthermore, inhibiting the HMGB1/RAGE axis significantly improved neurological outcomes in mice post-CA/CPR. These findings suggested aberrant activation of the HMGB1/RAGE axis after CA/CPR might contribute to the onset and progression of PCABI, and that therapeutic strategies targeting this signaling axis could exert a protective effect against PCABI.

Pharmacological inhibition of RAGE can mitigate myocardial IRI in rats [47]. Singh and Agrawal [34] showed that FPS treatment reduced the interaction between RAGE and its ligand HMGB1, thereby reducing HMGB1 expression. Thus, it reduced neuroinflammation and exerted a neuroprotective effect in ischemic brain injury [48]. FPS is highly effective, well-tolerated, and readily crosses the blood-brain barrier; it is therefore considered a novel therapeutic candidate with substantial translational potential [49]. Our findings demonstrated that FPS pretreatment suppressed the upregulation of the HMGB1/RAGE axis after CA. In addition, FPS administration significantly improved overall outcomes after CA, including increased survival, enhanced neurological recovery, and reduced body weight loss. Histological analyses further provided morphological evidence for its neuroprotective effects: H&E, Nissl, and FJB staining showed that FPS pretreatment attenuated structural damage, increased the number of surviving neurons, and reduced apoptotic cell death, indicating a marked reduction in neuronal degeneration and loss. In summary, this study emphasized that FPS, through modulation of the HMGB1/RAGE axis, might represent a potential therapeutic agent in mitigating IRI induced by CA.

Pyroptosis is a key contributor to the initiation and development of PCABI [50–52]. Once released extracellularly, either actively or passively, HMGB1 binds to RAGE receptors on macrophages, triggering a dynamic, receptor-mediated endocytosis. That then leads to inflammasome activation, pyroptosis, and the release of inflammatory mediators [26,53]. Based on these findings, our study investigated whether FPS pretreatment alleviated neuronal pyroptosis after CA/CPR by inhibiting the HMGB1/RAGE axis. Our results demonstrated that CA/CPR indeed induced significant neuronal pyroptosis in mice, as indicated by a marked upregulation of key pyroptosis-related proteins (cleaved caspase-1, GSDMD, N-GSDMD) and downstream inflammatory cytokines (IL-1β, IL-18). However, pretreatment with FPS downregulated these pyroptosis-related proteins and inflammatory cytokines. These findings collectively suggested that FPS pretreatment conferred neuroprotection after CA, at least in part by mitigating pyroptosis. However, the precise mechanistic link between the FPS-regulated HMGB1/RAGE axis and pyroptosis remains to be further elucidated through additional experiments.

At present, ROS-mediated oxidative stress is essential in PCABI [54,55]. The Nrf2 pathway has been shown to mitigate ROS-driven oxidative stress and improve neurological recovery after CA resuscitation [56–58]. RAGE activation may be closely associated with the accumulation of ROS in the nervous system [59]. FPS has been reported to inhibit NADPH oxidase activation and subsequent ROS production [60]. Consistent with previous findings, the present study showed that FPS notably upregulated the Nrf2/HO-1 antioxidant, reduced ROS accumulation, and alleviated oxidative stress after CA. However, this study did not include causal validation of the involved signaling pathways through *in vivo* gene-knockout experiments. Therefore, additional investigations are necessary to clarify the precise protective mechanism of FPS in PCABI.

This study had several limitations: (1) We evaluated the relationship between the action of FPS and pyroptosis after CA. However, we could not exclude the possibility that the HMGB1/RAGE pathway regulated by FPS may contribute to the modulation of other types of cell death. For instance, studies have demonstrated HMGB1/RAGE axis exacerbates myocardial IRI in mice by regulating apoptosis

and autophagy [53]. (2) We only investigated short-term changes to the HMGB1/RAGE pathway and the effect of FPS pretreatment after CA/CPR and did not assess long-term outcomes. Future studies should include additional long-term assessment time points (e.g., 7 and 14 days after CA) to systematically evaluate the dynamic changes associated with persistent activation of the HMGB1/RAGE axis and the sustained effects of FPS. Previous research has demonstrated that HMGB1 protein levels in rat hippocampus are significantly increased at 1 day after CA and continue to rise over the next 7 days [61], suggesting that this pathway may contribute to brain injury over a longer time. (3) The assessment of inflammation in the present study was not exhaustive. We only analyzed IL-18 and IL-1β levels, which are closely associated with pyroptosis, but did not characterize the broader network of inflammatory mediators downstream of the HMGB1/RAGE axis. However, studies have shown that activation of the HMGB1/RAGE axis leads to the upregulation of additional proinflammatory cytokines (e.g., IL-6 and tumor necrosis factor alpha [TNF-α]) via the classical pro-inflammatory NF-κB pathway, generating a positive feedback loop. This worsens pyroptosis by intensifying the inflammatory response and triggering inflammasome activation [13]. Therefore, future studies should incorporate additional lines of evidence, such as measurements of TNF-α, IL-6, NF-κB activation, and other downstream mediators, to comprehensively characterize the HMGB1/RAGE axis-driven inflammatory network and delineate its role in PCABI. (4) FPS was administered prior to CA in the present study, which represented a pretreatment paradigm and did not fully recapitulate clinical practice, where interventions are typically initiated after ROSC. Therefore, our findings should be interpreted primarily as pharmacological proof-of-concept supporting the HMGB1/RAGE axis as a druggable pathway in PCABI. Future studies should determine the therapeutic time window and optimal regimen for post-ROSC administration (e.g., different treatment delays and repeated dosing) to strengthen translational relevance.

5. Conclusion

In summary, pretreatment with FPS in a CA model was found to exert neuroprotective function by regulating the HMGB1/RAGE axis. It attenuated oxidative stress and pyroptosis associated with PCABI, thereby reducing cerebral damage and improving neurological outcomes.

Availability of Data and Materials

The datasets used and analysed during the current study are available from the corresponding author on reasonable request.

Author Contributions

YZ and ZY conceived and designed the study. YZ, YW, and JH conducted the behavioral experiments and acquired the data. YZ, QL, LL, SX, and LPL participated in data acquisition and contributed to data analysis and interpretation. YZ drafted the manuscript. ZY, QL, LL, SX, and LPL critically revised the manuscript for important intellectual content. LPL and ZY supervised the study. All authors contributed to editorial changes in the manuscript. All authors read and approved the final manuscript. All authors have participated sufficiently in the work and agreed to be accountable for all aspects of the work.

Ethics Approval and Consent to Participate

All animals received approval from the Laboratory Animal Centre of Renmin Hospital Wuhan University Committee (No. March 4, 2025 [20250304]) and were performed in accordance with the institutional guidelines for the care and use of laboratory animals.

Acknowledgment

We appreciate Jianfei Sun for providing guidance on animal experiments and the support of BioRender.

Funding

This work received financial support from the National Natural Science Foundation of China (No. 81772039), the Knowledge Innovation Program of the Wuhan Municipal Science and Technology Bureau (No. 2022020801010474), and the “Chutian Talent Program” for healthcare professionals in Hubei Province (No. CZ2024020001).

Conflict of Interest

The authors declare no conflict of interest.

Supplementary Material

Supplementary material associated with this article can be found, in the online version, at https://doi.org/10.31083/JIN50023.

References

[1] Narayan SM, Wang PJ, Daubert JP. New Concepts in Sudden Cardiac Arrest to Address an Intractable Epidemic: JACC State-of-the-Art Review. Journal of the American College of Cardiology. 2019; 73: 70–88. https://doi.org/10.1016/j.jacc.2018.09.083.

[2] Benjamin EJ, Muntner P, Alonso A, Bittencourt MS, Callaway CW, Carson AP, *et al*. Heart Disease and Stroke Statistics-2019 Update: A Report From the American Heart Association. Circulation. 2019; 139: e56–e528. https://doi.org/10.1161/CIR.0000000000000659.

[3] Perkins GD, Neumar R, Hsu CH, Hirsch KG, Aneman A, Becker LB, *et al*. Improving Outcomes After Post-Cardiac Arrest Brain Injury: A Scientific Statement From the International Liaison Committee on Resuscitation. Circulation. 2024; 150: e158–e180. https://doi.org/10.1161/CIR.0000000000001219.

[4] Willie CK, Tzeng YC, Fisher JA, Ainslie PN. Integrative regulation of human brain blood flow. The Journal of Physiology. 2014; 592: 841–859. https://doi.org/10.1113/jphysiol.2013.268953.

[5] Sandroni C, Cronberg T, Sekhon M. Brain injury after cardiac arrest: pathophysiology, treatment, and prognosis. Intensive Care Medicine. 2021; 47: 1393–1414. https://doi.org/10.1007/s00134-021-06548-2.

[6] Callaway CW, Donnino MW, Fink EL, Geocadin RG, Golan E, Kern KB, *et al*. Part 8: Post-Cardiac Arrest Care: 2015 American Heart Association Guidelines Update for Cardiopulmonary Resuscitation and Emergency Cardiovascular Care. Circulation. 2015; 132: S465–S482. https://doi.org/10.1161/CIR.0000000000000262.

[7] Su J, Ren X, Yang X. Targeted Temperature Management after Resuscitation of Cardiac Arrest: A Review. Journal of Integrative Neuroscience. 2025; 24: 27177. https://doi.org/10.31083/JIN27177.

[8] Nielsen N, Wetterslev J, Cronberg T, Erlinge D, Gasche Y, Hassager C, *et al*. Targeted temperature management at 33°C versus 36°C after cardiac arrest. The New England Journal of Medicine. 2013; 369: 2197–2206. https://doi.org/10.1056/NEJMoa1310519.

[9] Dankiewicz J, Cronberg T, Lilja G, Jakobsen JC, Levin H, Ullén S, *et al*. Hypothermia versus Normothermia after Out-of-Hospital Cardiac Arrest. The New England Journal of Medicine. 2021; 384: 2283–2294. https://doi.org/10.1056/NEJMoa2100591.

[10] Tang D, Kang R, Zeh HJ, Lotze MT. The multifunctional protein HMGB1: 50 years of discovery. Nature Reviews. Immunology. 2023; 23: 824–841. https://doi.org/10.1038/s41577-023-00894-6.

[11] Wang S, Zhang Y. HMGB1 in inflammation and cancer. Journal of Hematology & Oncology. 2020; 13: 116. https://doi.org/10.1186/s13045-020-00950-x.

[12] Saha S, Buttari B, Panieri E, Profumo E, Saso L. An Overview of Nrf2 Signaling Pathway and Its Role in Inflammation. Molecules. 2020; 25: 5474. https://doi.org/10.3390/molecules25225474.

[13] Balança B, Desmurs L, Grelier J, Perret-Liaudet A, Lukaszewicz AC. DAMPs and RAGE Pathophysiology at the Acute Phase of Brain Injury: An Overview. International Journal of Molecular Sciences. 2021; 22: 2439. https://doi.org/10.3390/ijms22052439.

[14] Jangde N, Ray R, Rai V. RAGE and its ligands: from pathogenesis to therapeutics. Critical Reviews in Biochemistry and Molecular Biology. 2020; 55: 555–575. https://doi.org/10.1080/10409238.2020.1819194.

[15] Hudson BI, Lippman ME. Targeting RAGE Signaling in Inflammatory Disease. Annual Review of Medicine. 2018; 69: 349–364. https://doi.org/10.1146/annurev-med-041316-085215.

[16] Oda Y, Tsuruta R, Fujita M, Kaneda K, Kawamura Y, Izumi T, *et al*. Prediction of the neurological outcome with intrathecal high mobility group box 1 and S100B in cardiac arrest victims: a pilot study. Resuscitation. 2012; 83: 1006–1012. https://doi.org/10.1016/j.resuscitation.2012.01.030.

[17] Omura T, Kushimoto S, Yamanouchi S, Kudo D, Miyagawa N. High-mobility group box 1 is associated with neurological outcome in patients with post-cardiac arrest syndrome after out-of-hospital cardiac arrest. Journal of Intensive Care. 2016; 4: 37. https://doi.org/10.1186/s40560-016-0161-4.

[18] Shi X, Li M, Huang K, Zhou S, Hu Y, Pan S, *et al*. HMGB1 binding heptamer peptide improves survival and ameliorates brain injury in rats after cardiac arrest and cardiopulmonary resuscitation. Neuroscience. 2017; 360: 128–138. https://doi.org/10.1016/j.neuroscience.2017.07.052.

[19] Wang P, Zuo H, Shi H, Wang Z, Ren X, Shi J, *et al*. Gastrodin inhibits reactive astrocyte-mediated inflammation in hypoxic-ischemic brain damage through S100B/RAGE-Smad3 signaling. Acta Biochimica et Biophysica Sinica. 2025; 57: 955–967. https://doi.org/10.3724/abbs.2024235.

[20] Sun Y, Zhu X, Zhu K, Yu J, Cheng L, Hei M. High-mobility Group Box 1 Contributes to Hypoxic-Ischemic Brain Damage by Facilitating Imbalance of Microglial Polarization through RAGE-PI3K/Akt Pathway in Neonatal Rats. International Journal of Medical Sciences. 2022; 19: 2093–2103. https://doi.org/10.7150/ijms.78641.

[21] Li H, Wu W, Sun Q, Liu M, Li W, Zhang XS, *et al*. Expression and cell distribution of receptor for advanced glycation end-products in the rat cortex following experimental subarachnoid hemorrhage. Brain Research. 2014; 1543: 315–323. https://doi.org/10.1016/j.brainres.2013.11.023.

[22] Yu P, Zhang X, Liu N, Tang L, Peng C, Chen X. Pyroptosis: mechanisms and diseases. Signal Transduction and Targeted Therapy. 2021; 6: 128. https://doi.org/10.1038/s41392-021-00507-5.

[23] Burdette BE, Esparza AN, Zhu H, Wang S. Gasdermin D in pyroptosis. Acta Pharmaceutica Sinica. B. 2021; 11: 2768–2782. https://doi.org/10.1016/j.apsb.2021.02.006.

[24] Long J, Sun Y, Liu S, Yang S, Chen C, Zhang Z, *et al*. Targeting pyroptosis as a preventive and therapeutic approach for stroke. Cell Death Discovery. 2023; 9: 155. https://doi.org/10.1038/s41420-023-01440-y.

[25] Oladapo A, Jackson T, Menolascino J, Periyasamy P. Role of pyroptosis in the pathogenesis of various neurological diseases. Brain, Behavior, and Immunity. 2024; 117: 428–446. https://doi.org/10.1016/j.bbi.2024.02.001.

[26] Xu J, Jiang Y, Wang J, Shi X, Liu Q, Liu Z, *et al*. Macrophage endocytosis of high-mobility group box 1 triggers pyroptosis. Cell Death and Differentiation. 2014; 21: 1229–1239. https://doi.org/10.1038/cdd.2014.40.

[27] Jia C, Zhang J, Chen H, Zhuge Y, Chen H, Qian F, *et al*. Endothelial cell pyroptosis plays an important role in Kawasaki disease via HMGB1/RAGE/cathespin B signaling pathway and NLRP3 inflammasome activation. Cell Death & Disease. 2019; 10: 778. https://doi.org/10.1038/s41419-019-2021-3.

[28] Zhu K, Zhu X, Yu J, Chen L, Liu S, Yan M, *et al*. Effects of HMGB1/RAGE/cathespin B inhibitors on alleviating hippocampal injury by regulating microglial pyroptosis and caspase activation in neonatal hypoxic-ischemic brain damage. Journal of Neurochemistry. 2023; 167: 410–426. https://doi.org/10.1111/jnc.15965.

[29] Baird L, Yamamoto M. The Molecular Mechanisms Regulating the KEAP1-NRF2 Pathway. Molecular and Cellular Biology. 2020; 40: e00099-20. https://doi.org/10.1128/MCB.00099-20.

[30] Liu JX, Zheng D, Chen L, Chen S, Min JW. Nuclear Factor Erythroid 2-Related Factor 2 as a Potential Therapeutic Target in Neonatal Hypoxic-Ischemic Encephalopathy. Journal of Integrative Neuroscience. 2024; 23: 103. https://doi.org/10.31083/j.jin2305103.

[31] Campbell NK, Fitzgerald HK, Dunne A. Regulation of inflammation by the antioxidant haem oxygenase 1. Nature Reviews. Immunology. 2021; 21: 411–425. https://doi.org/10.1038/s41577-020-00491-x.

[32] Hu Q, Zuo T, Deng L, Chen S, Yu W, Liu S, *et al*. β-Caryophyllene suppresses ferroptosis induced by cerebral ischemia reperfusion via activation of the NRF2/HO-1 signaling pathway in MCAO/R rats. Phytomedicine. 2022; 102: 154112. https://doi.org/10.1016/j.phymed.2022.154112.

[33] Yuan Z, Lu L, Lian Y, Zhao Y, Tang T, Xu S, *et al*. AA147 ameliorates post-cardiac arrest cerebral ischemia/reperfusion injury through the co-regulation of the ATF6 and Nrf2 signal-

ing pathways. Frontiers in Pharmacology. 2022; 13: 1028002. https://doi.org/10.3389/fphar.2022.1028002.
[34] Singh H, Agrawal DK. Therapeutic Potential of Targeting the HMGB1/RAGE Axis in Inflammatory Diseases. Molecules. 2022; 27: 7311. https://doi.org/10.3390/molecules27217311.
[35] Shen C, Ma Y, Zeng Z, Yin Q, Hong Y, Hou X, *et al*. RAGE-Specific Inhibitor FPS-ZM1 Attenuates AGEs-Induced Neuroinflammation and Oxidative Stress in Rat Primary Microglia. Neurochemical Research. 2017; 42: 2902–2911. https://doi.org/10.1007/s11064-017-2321-x.
[36] Hong Y, Shen C, Yin Q, Sun M, Ma Y, Liu X. Effects of RAGE-Specific Inhibitor FPS-ZM1 on Amyloid-β Metabolism and AGEs-Induced Inflammation and Oxidative Stress in Rat Hippocampus. Neurochemical Research. 2016; 41: 1192–1199. https://doi.org/10.1007/s11064-015-1814-8.
[37] Liu H, Yu Z, Li Y, Xu B, Yan B, Paschen W, *et al*. Novel Modification of Potassium Chloride Induced Cardiac Arrest Model for Aged Mice. Aging and Disease. 2018; 9: 31–39. https://doi.org/10.14336/AD.2017.0221.
[38] Wang L, Zhao D, Wang H, Wang L, Liu X, Zhang H. FPS-ZM1 inhibits LPS-induced microglial inflammation by suppressing JAK/STAT signaling pathway. International Immunopharmacology. 2021; 100: 108117. https://doi.org/10.1016/j.intimp.2021.108117.
[39] Ousta A, Piao L, Fang YH, Vera A, Nallamothu T, Garcia AJ III, *et al*. Microglial Activation and Neurological Outcomes in a Murine Model of Cardiac Arrest. Neurocritical Care. 2022; 36: 61–70. https://doi.org/10.1007/s12028-021-01253-w.
[40] Shen Y, Yan B, Zhao Q, Wang Z, Wu J, Ren J, *et al*. Aging Is Associated With Impaired Activation of Protein Homeostasis-Related Pathways After Cardiac Arrest in Mice. Journal of the American Heart Association. 2018; 7: e009634. https://doi.org/10.1161/JAHA.118.009634.
[41] Allen CP, Bird JD, Sekhon MS. The dynamic pathophysiology of post cardiac arrest brain injury: "time is brain". Current Opinion in Critical Care. 2025; 31: 123–130. https://doi.org/10.1097/MCC.0000000000001246.
[42] Kalogeris T, Baines CP, Krenz M, Korthuis RJ. Ischemia/Reperfusion. Comprehensive Physiology. 2016; 7: 113–170. https://doi.org/10.1002/cphy.c160006.
[43] Tanaka T, Narazaki M, Kishimoto T. IL-6 in inflammation, immunity, and disease. Cold Spring Harbor Perspectives in Biology. 2014; 6: a016295. https://doi.org/10.1101/cshperspect.a016295.
[44] Lotze MT, Tracey KJ. High-mobility group box 1 protein (HMGB1): nuclear weapon in the immune arsenal. Nature Reviews. Immunology. 2005; 5: 331–342. https://doi.org/10.1038/nri1594.
[45] Yang DB, Dong XQ, Du Q, Yu WH, Zheng YK, Hu W, *et al*. Clinical relevance of cleaved RAGE plasma levels as a biomarker of disease severity and functional outcome in aneurysmal subarachnoid hemorrhage. Clinica Chimica Acta. 2018; 486: 335–340. https://doi.org/10.1016/j.cca.2018.08.036.
[46] Wang J, Jiang Y, Zeng D, Zhou W, Hong X. Prognostic value of plasma HMGB1 in ischemic stroke patients with cerebral ischemia-reperfusion injury after intravenous thrombolysis. Journal of Stroke and Cerebrovascular Diseases. 2020; 29: 105055. https://doi.org/10.1016/j.jstrokecerebrovasdis.2020.105055.
[47] Bucciarelli LG, Kaneko M, Ananthakrishnan R, Harja E, Lee LK, Hwang YC, *et al*. Receptor for advanced-glycation end products: key modulator of myocardial ischemic injury. Circulation. 2006; 113: 1226–1234. https://doi.org/10.1161/CIRCULATIONAHA.105.575993.
[48] Shen L, Zhang T, Yang Y, Lu D, Xu A, Li K. FPS-ZM1 Alleviates Neuroinflammation in Focal Cerebral Ischemia Rats via Blocking Ligand/RAGE/DIAPH1 Pathway. ACS Chemical Neuroscience. 2021; 12: 63–78. https://doi.org/10.1021/acschemneuro.0c00530.
[49] Yang F, Wang Z, Zhang JH, Tang J, Liu X, Tan L, *et al*. Receptor for advanced glycation end-product antagonist reduces blood-brain barrier damage after intracerebral hemorrhage. Stroke. 2015; 46: 1328–1336. https://doi.org/10.1161/STROKEAHA.114.008336.
[50] Wu C, Diao M, Yu S, Xi S, Zheng Z, Cao Y, *et al*. Gut Microbial Tryptophan Metabolism Is Involved in Post-Cardiac Arrest Brain Injury via Pyroptosis Modulation. CNS Neuroscience & Therapeutics. 2025; 31: e70381. https://doi.org/10.1111/cns.70381.
[51] Sun Y, Li J, Wu H, Zhao Z, Cong T, Li L, *et al*. GABA_B Receptor Activation Attenuates Neuronal Pyroptosis in Post-cardiac Arrest Brain Injury. Neuroscience. 2023; 526: 97–106. https://doi.org/10.1016/j.neuroscience.2023.06.001.
[52] Chang Y, Zhu J, Wang D, Li H, He Y, Liu K, *et al*. NLRP3 inflammasome-mediated microglial pyroptosis is critically involved in the development of post-cardiac arrest brain injury. Journal of Neuroinflammation. 2020; 17: 219. https://doi.org/10.1186/s12974-020-01879-1.
[53] Zeng M, Liang G, Yuan F, Yan S, Liu J, He Z. Macrophages-derived high-mobility group box-1 protein induces endothelial progenitor cells pyroptosis. iScience. 2024; 27: 110996. https://doi.org/10.1016/j.isci.2024.110996.
[54] Hackenhaar FS, Medeiros TM, Heemann FM, Behling CS, Putti JS, Mahl CD, *et al*. Therapeutic Hypothermia Reduces Oxidative Damage and Alters Antioxidant Defenses after Cardiac Arrest. Oxidative Medicine and Cellular Longevity. 2017; 2017: 8704352. https://doi.org/10.1155/2017/8704352.
[55] Glantzounis GK, Salacinski HJ, Yang W, Davidson BR, Seifalian AM. The contemporary role of antioxidant therapy in attenuating liver ischemia-reperfusion injury: a review. Liver Transplantation. 2005; 11: 1031–1047. https://doi.org/10.1002/lt.20504.
[56] Uruno A, Yamamoto M. The KEAP1-NRF2 system and neurodegenerative diseases. Antioxidants & Redox Signaling. 2023; 38: 974–988. https://doi.org/10.1089/ars.2023.0005.
[57] Ahn JH, Lee TK, Kim DW, Shin MC, Cho JH, Lee JC, *et al*. Therapeutic Hypothermia after Cardiac Arrest Attenuates Hindlimb Paralysis and Damage of Spinal Motor Neurons and Astrocytes through Modulating Nrf2/HO-1 Signaling Pathway in Rats. Cells. 2023; 12: 414. https://doi.org/10.3390/cells12030414.
[58] Zhao Y, Yao Z, Lu L, Xu S, Sun J, Zhu Y, *et al*. Carbon monoxide-releasing molecule-3 exerts neuroprotection effects after cardiac arrest in mice: A randomized controlled study. Resuscitation Plus. 2024; 19: 100703. https://doi.org/10.1016/j.resplu.2024.100703.
[59] Piras S, Furfaro AL, Domenicotti C, Traverso N, Marinari UM, Pronzato MA, *et al*. RAGE Expression and ROS Generation in Neurons: Differentiation versus Damage. Oxidative Medicine and Cellular Longevity. 2016; 2016: 9348651. https://doi.org/10.1155/2016/9348651.
[60] Qiao X, Li W, Zheng Z, Liu C, Zhao L, He Y, *et al*. Inhibition of the HMGB1/RAGE axis protects against cisplatin-induced ototoxicity via suppression of inflammation and oxidative stress. International Journal of Biological Sciences. 2024; 20: 784–800. https://doi.org/10.7150/ijbs.82003.
[61] Xu M, Zhou GM, Wang LH, Zhu L, Liu JM, Wang XD, *et al*. Inhibiting High-Mobility Group Box 1 (HMGB1) Attenuates Inflammatory Cytokine Expression and Neurological Deficit in Ischemic Brain Injury Following Cardiac Arrest in Rats. Inflammation. 2016; 39: 1594–1602. https://doi.org/10.1007/s10753-016-0395-2.